RESEARCH ARTICLE

Hawkmoth flight stability in turbulent vortex streets

Victor Manuel Ortega-Jimenez[1,*], Jeremy S. M. Greeter[1], Rajat Mittal[2] and Tyson L. Hedrick[1,*]

[1]Department of Biology, University of North Carolina at Chapel Hill, Chapel Hill, NC 27599, USA and [2]Department of Mechanical Engineering, Johns Hopkins University, Baltimore, MD 21218, USA

*Authors for correspondence (vortega@berkeley.edu; thedrick@bio.unc.edu)

SUMMARY

Shedding of vortices is a common phenomenon in the atmosphere over a wide range of spatial and temporal scales. However, it is unclear how these vortices of varying scales affect the flight performance of flying animals. In order to examine these interactions, we trained seven hawkmoths (*Manduca sexta*) (wingspan ~9 cm) to fly and feed in a wind tunnel under steady flow (controls) and in the von Kármán vortex street of vertically oriented cylinders (two different cylinders with diameters of 10 and 5 cm) at speeds of 0.5, 1 and 2 m s^{-1}. Cylinders were placed at distances of 5, 25 and 100 cm upstream of the moths. Moths exhibited large amplitude yaw oscillations coupled with modest oscillations in roll and pitch, and slight increases in wingbeat frequency when flying in both the near (recirculating) and middle (vortex dominated) wake regions. Wingbeat amplitude did not vary among treatments, except at 1 m s^{-1} for the large cylinder. Yaw and roll oscillations were synchronized with the vortex shedding frequencies in moths flying in the wake of the large cylinder at all speeds. In contrast, yaw and pitch were synchronized with the shedding frequency of small vortices at speeds ≤1 m s^{-1}. Oscillations in body orientation were also substantially smaller in the small cylinder treatment when compared with the large cylinder, regardless of temporal or non-dimensional spatial scale. Moths flying in steady conditions reached a higher air speed than those flying into cylinder wakes. In general, flight effects produced by the cylinder wakes were qualitatively similar among the recirculating and vortex-dominated wake regions; the magnitude of those effects, however, declined gradually with downstream distance.

Supplementary material available online at http://jeb.biologists.org/lookup/suppl/doi:10.1242/jeb.089672/-/DC1

Key words: von Kármán vortex, *Manduca sexta*, unsteady flows, turbulence, stability, wind tunnel.

Received 15 April 2013; Accepted 2 September 2013

INTRODUCTION

Flying animals must overcome gusts, vortices and other disturbances in environmental flows, which results in deviations in orientation, position and direction. These perturbations are particularly challenging for insects and other small flying animals because the ratio of aerodynamic torque (approximately mass$^{4/3}$) to moment of inertia (approximately mass$^{5/3}$) increases with decreasing body size, making small animals potentially more subject to external aerodynamic perturbations (see Hedrick, 2011). The few existing studies in this area indicate that turbulence is an important factor for flying insects. For example, bees flying into a homogeneous turbulent air stream experience roll instabilities that are damped by extending their hind legs (Combes and Dudley, 2009). In general, complex environments can reveal important stability properties of animals and models of animal locomotion. For example, cockroaches running in rough terrain experience large changes in orientation, but with little effect on forward speed with minimal neural modulation, demonstrating the importance of visco-elastic mechanical feedback to locomotor stability (Sponberg and Full, 2008). Study of a pyramidal object supported by an oscillating flow revealed unexpected stability properties associated with periodic vortex shedding (Liu et al., 2012), indicating that complex environments do not necessarily produce destabilization.

Vortical flows are commonly found in natural fluid environments at a variety of scales (see Chopra and Hubert, 1965; Dritschel et al., 1999). For example, Poggi et al. (Poggi et al., 2004) found that

von Kármán vortex streets were the dominant flow structure found within a vegetative canopy below the mixing layer at the interface of the canopy and atmosphere, and elongate cylinders are known to readily form such vortex streets (e.g. Kawamura et al., 1984; Okamoto and Sunabashiri, 1992). The von Kármán vortex street is a ubiquitous unsteady flow structure that forms behind bluff bodies in flows (Williamson, 1996). These vortex streets are a result of an absolute instability mechanism of the wake (Ho and Huerre, 1984) and as such, they form rapidly and persist for large distances. While it is expected that natural flows will be more complex, the von Kármán vortex street is a useful and relevant model for studying how flying animals accommodate unsteady flows.

Curiously, despite recent advances in the knowledge of the costs (Webb, 1998) and the benefits (Liao et al., 2003a) of fish moving through these environmental vortical structures (for a review, see Liao, 2007), little is known about how flying animals deal with such perturbations. Trout swimming into large von Kármán vortices increase their tail beat amplitude by a factor of around three compared with free swimming; these tail strokes are synchronized with the vortex shedding (Liao et al., 2003b). Similarly, recent evidence suggests that hummingbirds flying in large vortex perturbations experience deviations in yaw, pitch and roll, with a consequent increase in metabolic rate (V.M.O.-J., N. Sapir, M. Wolf, E. Variano and R. Dudley, unpublished). Additionally, yaw effects experienced by hummingbirds were not at the vortex shedding frequency for vortices smaller than a wingspan. Thus, we predict

that the spatial scale will have a stronger influence on the observed perturbation magnitude than the temporal scale (i.e. vortex frequency) and that vortices with a spatial scale smaller than the wingspan of the animal will produce only small responses. Given the results from the trout studies, we expect that the moths will oscillate at the vortex shedding frequency within the range of 2 to 8 Hz examined here. All of these values are substantially below the typical wingbeat frequency of hawkmoths used in this study, which is approximately 28 Hz.

Vortex shedding behind a high-aspect-ratio circular cylinder begins at a Reynolds number (i.e. the dimensionless ratio between inertial and viscous forces, Re) (Vogel, 1994) of about 45 (Williamson, 1996). This vortex shedding is initially laminar, but undergoes a sequence of bifurcations beginning at around Re=180 that result in three-dimensional (3D) instabilities with an eventual transition to a turbulent wake at Re around 10^3. The Strouhal number [i.e. the dimensionless shedding frequency, St (Vogel, 1994)] in this Reynolds number regime is nearly constant at ~0.2 (Williamson, 1996). Additionally, velocity fluctuations in the vortex wake undergo an exponential decay in magnitude with downstream distance (Prasad and Williamson, 1997). Consequently, flying animals might experience greater control demands as they approach the origin of the shed vortices. We expect that these additional control requirements prevent hawkmoths from achieving the same flight speeds in the von Kármán vortices as they do in laminar flows, just as the control requirements for terrestrial locomotion over rough terrain reduce maximum speed in cockroaches (Sponberg and Full, 2008).

The flow perturbations (i.e. 3D instabilities and turbulence) in the von Kármán vortex wake of a circular cylinder are a function of the Reynolds number and the normalized downstream distance x/D, where x is the distance measured from the cylinder downstream edge and D is the cylinder diameter. For Reynolds numbers ranging from 10^3 to 10^4 (the range studied here), the fluctuations in the streamwise velocity reach a maximum that is roughly 45% of the free-stream velocity at x/D~1.5 and then decay rapidly (down to ~25% of free-stream velocity) by x/D~3.5 and then more slowly beyond that. The transverse velocity fluctuations reach a maximum at x/D~1.5 but the intensity of these fluctuations is higher, nearly 70% of the free-stream velocity (Parnaudeau et al., 2008). It should also be noted that streamwise velocity fluctuations near the wake centerline occur at twice the Strouhal frequency whereas the transverse velocity fluctuations occur at the Strouhal frequency. Moreover, at subcritical regimes it has been observed that vortex formation length is reduced with increasing Re (Williamson, 1996), and this implies a reduced recirculation zone. Thus, we predict that moths flying in the recirculation zone at x/D <3 will experience the greatest flight effects, and that the effect of transverse perturbations will be more evident than that of streamwise perturbations, whereas those flying beyond x/D >5 will experience a significantly reduced response magnitude. Streamwise flow perturbations are expected to produce effects in pitch while transverse flows perturbations will affect yaw and roll. All of these expected flight effects might be mitigated by control responses of the animal, but we expect this to affect the absolute rather than relative magnitude of the observed effect of different flow perturbation regimes.

Here we examine the effects of vortex spatial scale, temporal scale and wake region on flying animals by quantifying the flight effects in wing kinematics and body displacement experienced by hawkmoths flying in a wind tunnel in von Kármán vortex streets of varying scale, airspeed and distance from the vortex source.

MATERIALS AND METHODS
Moth training
We sampled seven male hawkmoths (*Manduca sexta* L.) with a body mass (m_b) of 1.3±0.2 g (mean ± s.d.), a body length (l_b) of 4.6±0.4 cm, a wing length (R_w) of 4.1±0.4 cm, a wingspan (b) of 9.0±0.5 cm and a one-wing area (S_1) of 6.9±0.8 cm^2. All individuals were taken as pupae from a colony maintained in the Department of Biology at the University of North Carolina at Chapel Hill (UNC-CH). After eclosure, moths were placed in separate cloth mesh cages (30×30×30 cm) and left for 3 to 4 days. Caged moths were provided with water *ad libitum* and the cages were kept inside of a controlled environmental room with a light:dark ratio of 4:1 over a period of 24 h. The extended light period was applied to reduce the rate at which the moths accumulate wing damage in the enclosures. Wing tip damage varied from 0 to ~10% of wing length; the wing area loss was less than 5%.

Following this post-eclosure period, moth training was initiated; moths were moved to the working section (0.6×0.6×1.1 m) of the wind tunnel (see Appendix, Wind tunnel characteristics). An artificial feeder, constructed from a plastic pipette tip, was placed in the middle of the working section. The feeder was filled with artificial nectar composed of ~75% tap water, ~20% sugar and ~5% honey. Rose flowers were collected from the UNC-CH campus to provide floral odor and to increase the feeding response of the moths (see below).

Flight training was initiated by placing a moth on the feeder. When a moth started to shiver its wings, the flowers were placed below the insect. At that time, most moths extended their proboscis and started to touch the feeder. However, if a moth failed to extend its proboscis it was returned to the holding cage for one or two more days and then checked for proboscis extension again. Shortly after touching the feeder, the moths typically began to fly erratically about the wind tunnel. Once the moth slowed down and began hovering steadily, we placed the flowers below it. Moths that attempted to feed from the flowers were then led to the artificial feeder. Immediately after the moth touched the feeder we removed the flowers. After several minutes of feeder exploration, the moth finally started to feed by inserting its proboscis into the feeder. Moths were fed in this way at least twice in the first training day. In some cases, as an alternative to fresh rose flowers, we used a cotton-tipped applicator soaked with nectar to guide the moth to the feeder. Trained moths almost immediately found the feeder and began to feed, even without the flower stimulus, once placed in the wind tunnel. The following day we used a small amount of nectar in the feeder to stimulate more feeding bouts, but this time we turned on the wind tunnel at different speeds (0.5, 1 and 2 m s^{-1}). On the third day we added the cylinders to the training environment, and allowed the moths to experience a vortex wake prior to conducting recordings.

Cylinders and von Kármán vortex street
We produced a von Kármán vortex street in the wind tunnel by placing a cylinder vertically spanning the working section upstream of the moth; we used cylinders of 5 cm (small) and 10 cm (large) diameter with a length of 55 cm. The feeder was placed in a fixed position in the wind tunnel working section at the approximate lateral and vertical midpoints (Fig. 1). In order to examine how downstream distance affected flight performance, we placed the feeder at 5, 25 and 100 cm (only for the large cylinder) downstream from the cylinder as measured from its downstream edge; thus the x/D ratios were 1 and 5 for the small cylinder and 0.5, 2.5 and 10 for the large cylinder.

Each moth flew in each vortex wake at flow speeds of 0.5, 1.0 and 2.0 m s^{-1} (only for x/D greater than 1) (see Tables 1 and 2 for vortex treatments and shedding characteristics). Thus, 15 treatments with
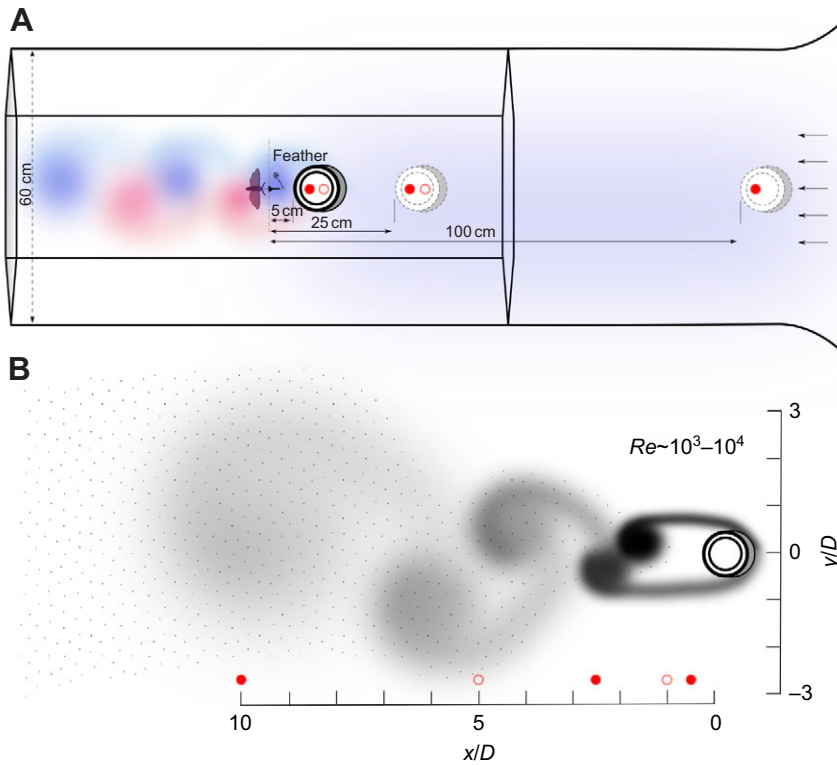
Fig. 1. (A) Top view of the experimental setup used to study the effects of vortex wakes on the flight of *Manduca sexta*, showing the working section of the wind tunnel, a portion of the nozzle and the position of the moth and cylinders. Note that the cylinder wake shown here is only a general representation of the von Kármán vortices produced in the experiments. The moth, tunnel and cylinders are to scale. (B) Schematic representation of the vortex shedding structure at Re ~10^3–10^4 in relation to x/D (i.e. downstream distance normalized to cylinder diameter). Filled and unfilled red circles represent large and small cylinders, respectively. Note how vortex decay increases with distance (for details, see Parnaudeau et al., 2008).

varying cylinder size, flow speed and downstream distances and four control treatments were used (Table 1). Note that the control at 3 m s^{-1} speed was only to examine whether the moth could fly at a higher speed in a steady flow than the maximal speed reached during treatments with cylinders; no moth was able to fly at this speed behind a cylinder with the feeder 25 cm downstream. All sampled moths were able to fly at 3 m s^{-1} under steady airflow conditions.

Video recordings

We recorded the feeding flights with three high-speed cameras (two Phantom v7.1, one Phantom v5.1, Vision Research Inc., Wayne, NJ, USA) equipped with 35 mm lenses and operating at 250 frames s^{-1}. Illumination was provided by two 12 W multi-LED infrared (730 nm) lights (Larson Electronics LLC, Kemp, TX, USA) placed laterally and a 10 W desk lamp placed on the top of the tunnel. One camera was placed directly above the feeding location to an overhead view; the other two cameras were placed laterally, providing left and right oblique views. The cameras were calibrated from a calibration frame using direct linear transformation (DLT) (Abdel-Aziz and Karara, 1971). Recordings were collected under the following experimental conditions shown in Table 1: control (no cylinder present), and cylinder treatments that include different combinations of cylinder size, airspeed and downstream distance (see above and Table 1 for details).

Table 1. Moth orientation angle oscillation amplitudes and wingbeat frequency under varied vortex perturbation conditions

Treatment	x/D	ψ (deg)	θ (deg)	ϕ (deg)	η_w (Hz)	φ_A (deg)
0.5 m s^{-1}						
Control	–	4.4±1.1	7.7±2.7	5.9±2.3	27.8±1.2	85.7±5.5
Large cylinder	0.5	35.4±3.4	9.8±1.4	8.9±2.2	28.6±1.3	83.2±3.8
	2.5	20.6±3.8	12.2±2.0	7.7±1.7	28.0±1.2	84.3±4.9
	10	6.6±1.9	8.6±2.5	6.0±1.6	28.0±0.9	84.9±4.2
Small cylinder	1	11.0±1.2	7.6±1.1	6.3±1.6	28.5±1.2	84.3±4.1
	5	13.4±2.1	8.5±2.1	7.1±1.3	27.5±1.5	84.4±5.3
1 m s^{-1}						
Control	–	4.6±2.1	7.5±2.9	5.5±1.5	27.4±1.7	84.9±4.2
Large cylinder	0.5	54.1±12.1	19.4±10.4	17.7±4.4	29.7±1.2	80.6±4.0
	2.5	42.9±10.4	13.5±4.4	13.8±3.0	28.3±1.5	81.9±4.0
	10	7.4±1.8	7.9±2.1	7.6±1.9	27.3±1.0	85.0±5.8
Small cylinder	1	16.6±5.8	10.7±2.6	11.7±3.6	28.5±1.1	82.2±5.6
	5	14.9±2.1	9.8±1.7	11.9±2.4	27.2±1.4	81.7±4.4
2 m s^{-1}						
Control	–	5.2±2.0	9.6±3.6	10.2±5.5	27.5±2.2	79.2±5.3
Large cylinder	2.5	57.3±10.4	23.0±4.1	37.7±8.5	28.8±1.9	81.9±4.7
Small cylinder	2.5	18.0±4.9	14.9±2.2	22.8±4.4	26.9±1.7	78.9±4.8
3 m s^{-1}	–					
Control	–	6.4±1.7	12±2.7	10.6±5.5	27.8±2.0	76.2±4.7

Data shown are means ± s.d. See details of measurements and calculations in the Materials and methods. N=7 moths in all cases.

Table 2. Moth orientation angle oscillation frequencies in vortex wakes produced by two cylinder sizes (5 and 10 cm diameter) at different speeds and positions, along with experimental characterization of vortex shedding frequencies

Treatment	x/D	Yaw (Hz)	Pitch (Hz)	Roll (Hz)	f_v (Hz)	f_F (Hz)	Re (×10³)	St
0.5 m s⁻¹								
Large cylinder	0.5	1.1±0.3	2.6±1.3	2.4±1.2				
	2.5	1.1±0.1	2.6±1.5	4.1±2.7	1.1±0.1		3.4	0.21±0.03
	10	2.8±1.8	3.3±1.2	4.5±0.8				
Small cylinder	1	2.0±0.4	3.8±0.8	3.7±1.2				
	5	2.1±0.2	2.4±1.2	3.7±2.1	2.0±0.1		1.7	0.20±0.03
1 m s⁻¹								
Large cylinder	0.5	2.0±0.7	2.7±2.5	2.4±0.4				
	2.5	2.1±0.1	1.1±0.6	2.1±0.9	2.2±0.1	1.9±0.2	6.8	0.22±0.03
	10	2.3±1.3	3.2±1.2	3.5±0.9				
Small cylinder	1	3.1±1.0	3.0±1.0	4.0±0.6				
	5	3.3±0.5	3.1±1.0	3.5±0.4	4.4±1.0	2.9±0.2	3.4	0.19±0.03
2 m s⁻¹								
Large cylinder	2.5	4.0±0.2	2.3±1.3	4.0±0.2	4.2±0.3	3.9±0.2	13.7	0.21±0.03
Small cylinder	5	3.0±1.6	3.3±1.6	6.1±1.8	8.2±0.5	6.4±1.2	6.8	0.21±0.03

Data shown are means ± s.d. See details of measurements and calculations in the Materials and methods. N=7 in all cases (except for Re).

Flow visualizations

We used the smoke-wire technique to visualize the cylinder wakes (see Marzkirch, 1987). We filmed smoke visualizations using one of the high-speed cameras described above and used the recording to measure the vortex shedding frequency (f_v) from the movement of the smoke vortices. The Strouhal number for each treatment was calculated as $St=f_vDU^{-1}$, where U is the airflow velocity. The Reynolds number for each vortex shedding was calculated as $Re=DU\upsilon^{-1}$, where υ is the kinematic viscosity ($1.46\times10^{-5}\,\mathrm{m^2\,s^{-1}}$; see Table 2). Additionally, we recorded the smoke visualization with a moth flying in the wake generated by the large (10 cm) and small (5 cm) cylinders at 1 m s⁻¹ and downstream distance of 5, 25 and 100 cm (only for the 10 cm cylinder). The moths typically retracted their proboscis from the feeder and left the recording region once they detected the smoke, limiting the duration of these recordings. Thus, only one moth was filmed with the smoke visualization flying at 1 m s⁻¹ in the large and small cylinder wakes.

As vortex instabilities are common in the airflow regimes used here, we used a freely oscillating bird feather placed in the vortex street to see whether the moth body oscillations are in synchrony with those of the vortex shedding. The feather length was 10 cm and it was placed at a height of 22 cm from the bottom of the working section. The feather was positioned below the feeder during all video recording for each treatment with the cylinder positioned at a distance of 25 cm. Finally, we collected smoke visualizations to verify that the feather oscillations were in phase with the vortex shedding in the cylinder's wake. Feather oscillation frequencies (f_F) were calculated from the above video recordings with moths. However, smoke visualizations of feathers at 0.5 m s⁻¹ showed little oscillation response with the vortex shedding; thus we excluded those feather data from the analysis of those speeds.

Smoke visualization revealed shear layer instabilities and turbulence during all wake and speed conditions. Occasionally we observed an interaction between alternate vortices, giving rise to instabilities in shedding frequency. Qualitatively, the vortex size in the near wake (x/D=2.5 and 5) resembles that of each cylinder (see supplementary material Movie 6). At 2 m s⁻¹ vortices appeared to be rotated with a slight tilt. Smoke visualization of the bird feather indicated that it oscillates passively in synchrony with the vortices (supplementary material Movie 1). However, as the feather was placed ~10 cm below the moth, the downward flow produced by the flapping wings might have also affected the feather oscillation, particularly for the small cylinder treatments (supplementary material Movie 4).

Smoke visualization showed that both wings interacted with the large cylinder's wake. In contrast, in the small cylinder treatment the incoming vortices interacted mostly with only one wing at a time (supplementary material Movie 6). The decay of the large vortex wake was clearly visible at 100 cm downstream (x/D=10). At this downstream distance a distinct vortex structure was unrecognizable and the streakiness indicates a turbulent airstream.

3D reconstruction and kinematic calculations

The resulting videos were analyzed by first using an entropy filter to segment the image and isolate the moth from the background. Following segmentation, the total pixel area and pixel coordinates [p_x,p_y] of the moth silhouette extrema, e.g. the moth p_x coordinate at maximum moth p_y (Fig. 2A), were collected from each frame of each camera. The wingbeat frequency was measured from the power spectrum of the fluctuations in total moth pixel area in the overhead camera (Fig. 2B). Because the pixel area fluctuates regularly through each wingbeat cycle, the greatest signal power was present at the moth's average wingbeat frequency, η_w. Next, a Hilbert transform was used to identify the frames corresponding to a particular phase in the wingbeat cycle (mid-downstroke) from the pixel area measurement (Fig. 2C). The left and right extrema of each video image were automatically collected and combined with the DLT coefficients to reconstruct the 3D position of the left and right wing tips.

Secondly, we filtered the silhouette images in the time domain by selecting only pixels which appeared in the moth in video frames n–2, n and n+2, where n is the frame of interest. Because the wings move rapidly compared with the body, head and abdomen, this operation isolates the body pixels from the wing pixels. A set of pixel erosion followed by dilation operations was then used to remove thin extremities such as the antenna and proboscis from the filtered silhouette. The anterior and posterior silhouette extrema and silhouette centroid were then automatically identified in all three cameras and used to reconstruct the 3D position of the head, tip of the abdomen and body centroid, respectively, using the DLT coefficients. In cases of large body yaw, this body alignment was used to rotate the segmented pixel arrays into a standard position prior to wing tip identification. These position time series were then
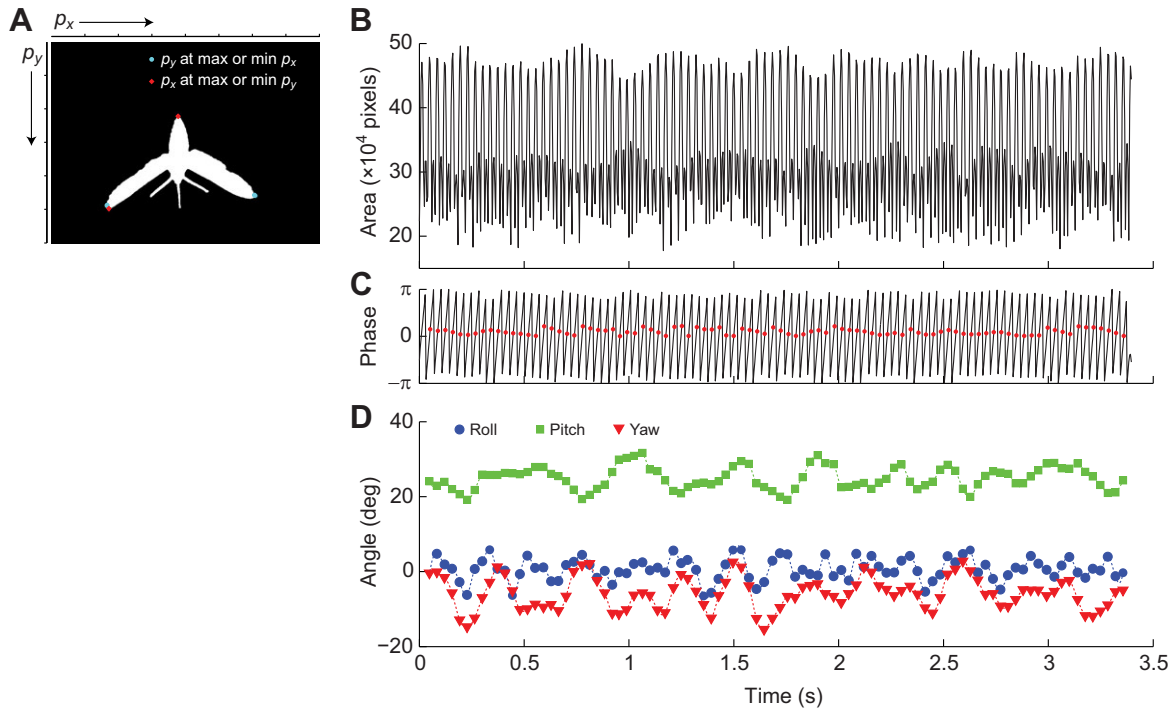
A

B

C

D

Fig. 2. (A) An example of a moth video frame following video processing. The moth, shown here as a silhouette, was separated from the background using an entropy filter, then the pixel coordinate extrema within the silhouette were identified, shown here as red diamonds and cyan circles. (B) Total pixel area varies through the wingbeat cycle. (C) Video frames at identical phases were automatically identified by applying a Hilbert transform to the pixel area data; mid-downstroke instants are indicated by red circles. (D) Roll, pitch and yaw orientation were then measured at each mid-downstroke instant. Image and kinematic data shown are from a small cylinder recording at $1\,\mathrm{m\,s^{-1}}$, x/D=5.

examined for reconstruction artifacts, defined as points with DLT residuals two standard deviations greater than the mean residual for that point. These points (5.2% of the total) were removed and the gaps linearly interpolated. Next, the 3D positions were subjected to a 60 Hz (~2× wingbeat frequency) low pass fourth-order zero-lag digital Butterworth filter.

The yaw, pitch and roll orientation of the moth with respect to the inertial coordinate system was then determined at each mid-downstroke from the position of the head, abdomen tip, left wing tip and right wing tip following a yaw, pitch, roll order for transformation from the wind tunnel frame to the body frame (Fig. 3). From these data, we linearly interpolated the yaw, pitch and roll angles between successive mid-downstroke events to provide a continuous orientation measure while accounting for the slight non-uniform temporal spacing of the mid-downstroke events (Fig. 2D). The dominant oscillation frequency and amplitude of each of the orientation angles was extracted *via* power spectrum analysis. Note that no further low pass filters were applied to the kinematic data, but the mid-downstroke to mid-downstroke reconstruction routine implicitly filters the data at wingbeat frequency, ~26 Hz here.

In addition to body orientations, we examined wingbeat amplitude given by the 3D wingtip positions and body centroid at the beginning and end of each downstroke. Wingbeat amplitude was measured as the angle between the vectors running from the body centroid to the wing tip at the start of downstroke and the end of downstroke. Body pitch and wingbeat amplitude were not correctly calculated by the automated analysis routines for the $2\,\mathrm{m\,s^{-1}}$ large cylinder trials and for one $2\,\mathrm{m\,s^{-1}}$ control because of the large-amplitude body oscillations moving the image extrema from their expected locations; these were supplemented by manual digitization of the right wing tip and abdomen tip (Hedrick, 2008). This set of

automated video analysis routines permitted examination of 195,780 frames and 7421 wingbeat cycles in total. The automated video analysis routines produced estimated spatial errors of [0.013±0.009, 0.017±0.012, 0.012±0.009 cm] (mean ± s.d.) for the body points and [0.161±0.119, 0.210±0.156, 0.167±0.138 cm] for the wing tips in the inertial [X, Y, Z] coordinate system. In subsequent statistical analysis we used the average body oscillation amplitudes (roll, ϕ; pitch, θ; and yaw, ψ), the average wingbeat frequency (η_w) and
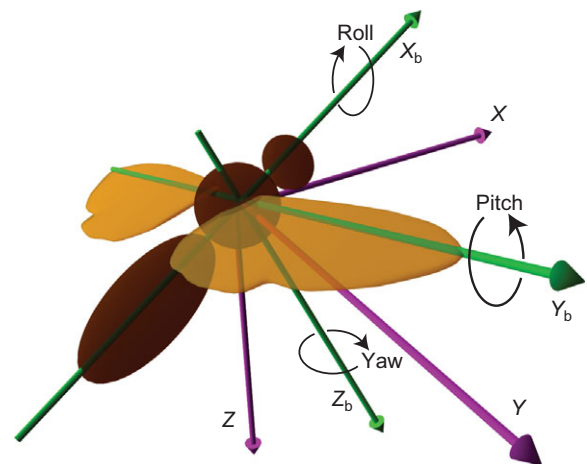

Fig. 3. Inertial frame (X-Y-Z) and body (X_b-Y_b-Z_b) axes used to calculate the yaw, pitch and roll orientation of the moth. Roll, pitch and yaw are a series of ordered rotations about the body axes that shift the body axes from an orientation aligned with the inertial frame axes to the observed orientation. We used a yaw, pitch, roll rotation order in this study; this order minimizes the calculated yaw magnitude.

Table 3. Repeated-measures ANOVA and Kruskal–Wallis analysis of kinematics and oscillation frequencies at each tested airspeed

Variable	Speed (m s^{-1})	d.f.	Test statistic	P
Wingbeat frequency	0.5	5,30	F=1.7	0.18
	1	5,30	F=10.2	<0.001
	2	2,12	F=7.1	0.009
Wingbeat amplitude	0.5	5,30	F=0.97	0.5
	1	5,30	F=5.3	0.01
	2	2,12	F=2.14	0.2
Yaw amplitude	0.5	5,30	F=87.9	<0.001
	1	5,30	F=141.9	<0.001
	2	2,12	F=139.4	<0.001
Pitch amplitude	0.5	5,30	F=5.4	0.001
	1	5,30	F=6.4	0.007
	2	2,12	F=26.1	<0.001
Roll amplitude	0.5	5,30	F=5.15	0.002
	1	5,30	F=22.69	<0.001
	2	2,12	F=32.2	<0.001
Oscillation frequencies*	0.5 (small)	3	χ^2=8.15	0.04
	0.5 (large)	3	χ^2=12.12	0.007
	1 (small)	4	χ^2=11.75	0.019
	1 (large)	4	χ^2=19.27	<0.001
	2 (small)	4	χ^2=23.96	<0.001
	2 (large)	4	χ^2=17.31	0.0017

See Materials and methods for details. *Comparison between body oscillation, feather and vortex frequencies.

average wing amplitude angle (φ_A) from each trial. Uncertainty for each of these per-trial measurements was quantified by repeatedly re-running the analysis routines with additional spatial error of the aforementioned mean and standard deviation added to each point. The effect of the additional error was to change the resulting estimate of the wingbeat amplitudes along with the body oscillation frequencies and amplitudes for each resampled trial. We quantified these changes by computing the standard deviation of the set of resampled data; these were [1.6, 0.4, 0.4 Hz] for ϕ, θ and ψ oscillation frequency, [1.5, 0.3 and 0.2 deg] for the respective oscillation amplitudes and 1.4 deg for φ_A. We also examined whether the wing tip positions at mid-downstroke adequately represent the body roll angle by manually digitizing the left and right wing root position at mid-downstroke and using these inputs in place of the automatically digitized wing tip positions for a small subset of the data. Both versions of the analysis identified the same characteristic oscillation frequency and differed by 1.8 deg (18.6 *versus* 16.8) in roll oscillation amplitude. Video analysis and kinematics calculations were performed in MATLAB (The MathWorks, Natick, MA, USA).

Statistics

For each speed, ϕ, θ, ψ, η_w and φ_A were analyzed with RM-ANOVAs to compare each treatment (corresponding cylinder size × downstream distances) and controls at each speed. Pairwise comparisons were analyzed with a Tukey's *post hoc* test. Logarithmic transformations were applied for yaw (0.5 and 2 m s^{-1}), roll (2 m s^{-1}) and wingbeat frequency (2 m s^{-1}) in order to fulfill assumptions of normality and homogeneity of variance. Similarly, inverse logarithmic functions were applied to pitch, roll was raised to the power of 2/3 at 0.5 m s^{-1} and a double square root transformation was applied to yaw at 1 m s^{-1}. A Kruskal–Wallis test, followed by a Wilcoxon pairwise test, was used to compare f_v, f_F (except for 0.5 m s^{-1}) and the moth abdomen tip oscillation in yaw, pitch and roll for each cylinder treatment (cylinder size × speed). Mauchly tests for sphericity were significant for θ at 1 m s^{-1}; accordingly, we used the Huynh–Feldt correction. Moth abdomen tip frequencies (f_b) at 25 cm downstream were used for

comparisons. The influence of the yaw moment of inertia (I_{ZZ}) [see Hedrick et al. (Hedrick et al., 2009) for calculation details] on yaw oscillations was explored using linear fits, and a corresponding significant test for regression, for each speed and cylinder combination at 25 cm downstream. Linear regressions were used to identify overall trends in kinematic variables with the non-dimensional downstream distance x/D and tunnel flow speed. The statistical results are described in Tables 3–5.

Experimental and analytical limitations

The set of experimental and analytical procedures described above is limited by a number of factors. Without the use of particle image velocimetry we are unable to precisely visualize or quantify the precise interaction between the moths' wings and the incoming vortices and thus cannot determine the underlying aerodynamic effects that produce the body orientation oscillations we observed. Furthermore, the moths did not all choose to fly in the same exact location in the vortex stream, potentially increasing variability in the experimental results. Although the automated video analysis routines used here allow analysis of many images, they do not provide details sometimes calculated from manually digitized video such as the amount of long-axis rotation of the wing or the amount of wing deformation. Finally, because we did not collect any neuromuscular recordings from the moths we cannot demonstrate whether they exhibit any control responses when flying in the von Kármán vortex streets.

RESULTS
Wingbeat frequency and amplitude

In general, wingbeat frequency was inversely related to x/D (Fig. 4A, Table 4). Specifically, for the large cylinder at 1 m s^{-1}, moths flying at x/D=0.5 presented a η_w significantly higher than all other cases (P<0.01 for all pair comparisons), and this value was reduced proportionally at greater distances (x/D=2.5, 10; Table 4, supplementary material Movie 3). At those greater distances, η_w was similar to control flights (P>0.29 for both pair comparisons). However, only moths flying in the large cylinder's wake at x/D=2.5 (2 m s^{-1}) and 0.5 (1 m s^{-1}) increased their wingbeat frequencies
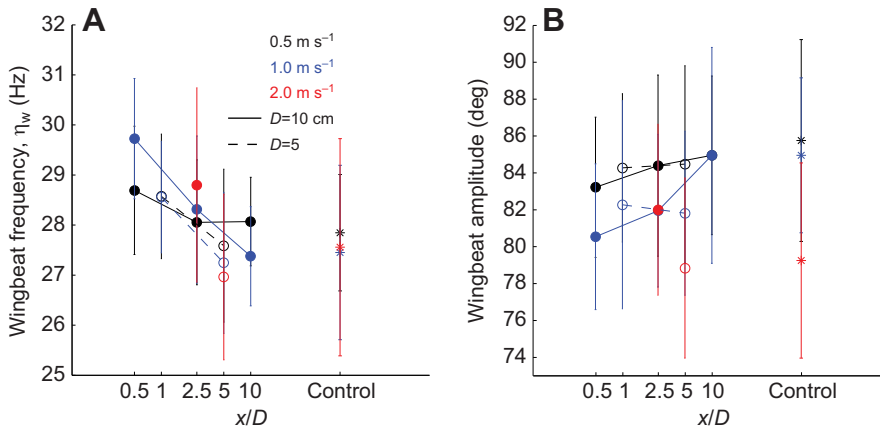
Fig. 4. Wing kinematics under varied vortex sizes, airspeeds and normalized downstream distances (x/D). Filled and open symbols represent the wakes from the large and small cylinder, respectively. Continuous and dashed lines represent the trend in the large and small cylinder data, respectively. Tested airspeeds are in red ($2\,\text{m s}^{-1}$), blue ($1\,\text{m s}^{-1}$) and black ($0.5\,\text{m s}^{-1}$). Controls are represented by asterisks. (A) Wingbeat frequency (η_w) *versus* x/D. (B) Wingbeat amplitude (φ_A) *versus* x/D. Error bars represent ±1 s.d.

compared with controls ($P<0.05$ for both comparisons). Similarly, for the small cylinder, η_w at shorter distance ($x/D=1$) was greater than at the larger distance ($x/D=5$), but neither differed significantly from controls at $1\,\text{m s}^{-1}$ ($x/D=1$, $P=0.08$; $x/D=5$, $P=0.99$; Fig. 4A, Table 1).

In contrast, wingbeat amplitude (Fig. 4B, Tables 1, 4) was unrelated to x/D, except at $1\,\text{m s}^{-1}$. At that speed, the wingbeat amplitude of moths flying behind the large cylinder at $x/D=0.5$ was significantly lower than that of the control ($P=0.001$).

Body orientation oscillations
Amplitude
On the whole, yaw oscillation amplitudes in the large cylinder treatment increased with increasing flow velocity (Table 5) and increasing x/D (Table 4); no trends were evident in the small cylinder treatment (Fig. 5A). Specifically, yaw oscillation amplitude for the large cylinder was inversely related to the downstream distance at 1 and $0.5\,\text{m s}^{-1}$ (Tables 1, 4, supplementary material Movie 3). All pair contrasts between distance treatments and controls of yaw were statistically different at 0.5 and $2\,\text{m s}^{-1}$ ($P<0.01$ for all pair combinations); at $1\,\text{m s}^{-1}$ we did not find differences in yaw oscillation amplitude among $x/D=0.5$ and 2.5 ($P=0.09$), but it was

slightly higher for $x/D=10$ compared with the control ($P=0.008$). Moths flying at 1 and $2\,\text{m s}^{-1}$ in the wake of the large cylinder at $x/D=0.5$ and 2.5, respectively, exhibited the highest yaw average amplitude, reaching up to 55 deg (Fig. 4A, supplementary material Movies 1, 2). In the small cylinder treatments we found that yaw did not differ among $x/D=1$ and 5 at either 1 or $0.5\,\text{m s}^{-1}$ ($P>0.5$ for both pairs), but nevertheless for those distances it was significantly higher than the respective controls ($P<0.001$ for all pair combinations; Fig. 5A). Yaw for the small cylinder was greatest at $2\,\text{m s}^{-1}$ and significantly greater than the respective control recordings ($P<0.001$; Table 1, supplementary material Movies 1, 4).

Overall, pitch oscillation amplitudes were smaller than those in yaw and significant effects were confined to a few cases (Fig. 5B). The pitch oscillation amplitude of the moths was affected by the large cylinder wake at $x/D=2.5$ at all speeds and at $x/D=0.5$ (only at $1\,\text{m s}^{-1}$) in comparison with controls ($P<0.01$ for all pair comparisons; Table 1). In contrast, the small cylinder wake influenced pitch oscillation amplitude only at the highest speed ($P=0.01$).

Trends in roll oscillation amplitude were similar on the whole to those in yaw, but with decreased magnitude and statistical significance (Fig. 5C, Table 4). The roll oscillation amplitude of

Table 4. Linear regression analysis of kinematic variables at two flight speed treatments in relation to non-dimensional downstream distance x/D from the large cylinder only and from both cylinders together

Variable	Cylinder	N	Speed (m s⁻¹)	Slope	Intercept	R^2	F	P
Wingbeat frequency	Large	21	0.5	−0.1	28.5	0.03	0.6	0.45
		21	1	−0.2	29.4	0.34	9.8	0.005
	Both	35	0.5	−0.1	28.4	0.04	1.21	0.27
		35	1	−0.2	29	0.24	10.3	0.003
Wingbeat amplitude	Large	21	0.5	0.2	83.5	0.02	0.5	0.49
		21	1	0.5	80.6	0.15	3.4	0.08
	Both	35	0.5	0.1	83.8	0.01	0.4	0.54
		35	1	0.4	80.9	0.1	2.7	0.11
Yaw amplitude	Large	21	0.5	−2.7	32.6	0.84	100.1	<0.001
		21	1	−4.9	55.9	0.84	102.1	<0.001
	Both	35	0.5	−2.0	24.8	0.43	24.7	<0.001
		35	1	−3.6	40.9	0.42	23.6	<0.001
Pitch amplitude	Large	21	0.5	−0.2	11.2	0.15	3.2	0.09
		21	1	−1.1	18.3	0.33	9.4	0.006
	Both	35	0.5	−0.1	9.7	0.02	0.7	0.4
		35	1	−0.8	15.5	0.21	9	0.005
Roll amplitude	Large	21	0.5	−0.3	8.8	0.32	8.9	0.01
		21	1	−1.0	17.5	0.64	33.6	<0.001
	Both	35	0.5	−0.2	7.9	0.12	4.6	0.04
		35	1	−0.8	15.6	0.4	21.3	<0.001

Only two x/D values were tested at a flight speed of $2\,\text{m s}^{-1}$, so we did not perform a regression for data from that speed.

Table 5. Linear regression analysis of kinematic variables *versus* flight speed, using pooled data from both cylinder sizes, all *x/D* and all flow speeds

Variable	Slope	Intercept	R^2	F	P
Wingbeat frequency	0.20	28.4	0.01	0.41	0.52
Wingbeat amplitude	−2.6	85.3	0.10	7.4	0.008
Yaw amplitude	13.7	11.7	0.15	15.0	<0.001
Pitch amplitude	6.4	6.0	0.32	38.5	<0.001
Roll amplitude	15.2	−1.3	0.70	190.9	<0.001

N=84.

moths flying at 0.5 m s^{-1} in the wake of the large cylinder at *x/D*=0.5 was significantly higher than that of controls and treatments at *x/D*=1 and 10 (*P*<0.01 for the three contrasts; Table 1). Meanwhile, at 1 m s^{-1} moths exhibited significantly larger roll oscillations than controls at *x/D* of 0.5, 1, 2.5 and 5 (*P*<0.001 for all contrast pairs). At 2 m s^{-1}, roll was greatest for the large cylinder between treatments (*P*<0.01 for all contrasts) and greater for the small cylinder treatment than in the control (*P*=0.001).

Moment of inertia (I_{zz}) and yaw amplitude were weakly correlated for both cylinders at all speeds (R^2<0.3 for all linear fits; $F_{1,5}$<1.7, *P*>0.05 for all cases), except for the large cylinder at 2 m s^{-1} [$f(x)$=−2.73×10^{8}x+96.7, R^2=0.76; $F_{1,5}$=15.8, *P*=0.01; Fig. 6]. In the case of the 1 m s^{-1}, large cylinder treatment (i.e. solid blue line in Fig. 6), a moth with a lower moment of inertia had a large effect on the yaw data; however, it was not enough to result in a significant correlation value between moment of inertia and yaw oscillation amplitude for this speed.

Frequency

We found that vortex shedding from the large cylinder was synchronized with the yaw oscillation frequency at all speeds (*P*>0.1 for the three contrasts), and with roll at 1 and 2 m s^{-1} (*P*>0.1 for both contrasts), but there was no pitch synchronization at any speed (*P*<0.05 for the three contrasts). In the small cylinder treatment, yaw and pitch frequencies matched the vortex shedding frequency at 0.5 m s^{-1}; at 1 m s^{-1}, yaw, pitch and roll matched (Wilcoxon test, *P*>0.002 for all comparisons). At 2 m s^{-1}, yaw, pitch and roll oscillations were at a significantly lower frequency (*P*<0.05 for all contrasts) than that of vortex shedding (Fig. 7). Feather oscillation frequencies were 10 and 25% significantly lower than those of the

vortex shedding for the large and small cylinder, respectively (Wilcoxon test, *P*<0.05).

DISCUSSION

Our results enable us to examine the relationship between the spatial and temporal scale of the fluid perturbation as well as the effect of airspeed and decay of von Kármán vortices on the responses of flying animals. In particular, vortex size and vortex decay appear to be the most important factors in explaining the observed kinematic effects on hawkmoths, and therefore might affect the energetics or ecology of flying animals. However, because of the small number of studies of animal locomotion in unsteady flows or over uneven terrain, these effects remain speculative.

Vortex size effects

Moth responses were clearly vortex size dependent. Body yaw and roll oscillation amplitudes and wingbeat frequency changes observed in moths were strongly associated with dimensional vortex size. Moths flying at *x/D*=0.5 in large cylinder vortex wakes exhibited yaw, pitch and roll oscillation amplitudes of ~60, 20 and 40 deg, respectively, and also presented wingbeat frequencies 10% higher than control flights. In contrast, moths flying in smaller vortices showed only moderate effects in yaw, pitch and roll angles, even at 2 m s^{-1}. These were lower than 30 deg at all *x/D* tested.

Smoke visualizations of the moth flying into the cylinder's wake showed that large vortices interact with both the left and right wings; meanwhile, small vortices interact mostly with one wing at a time (see Fig. 8, supplementary material Movie 6). This suggests that vortices with a size smaller than one wingspan could be less
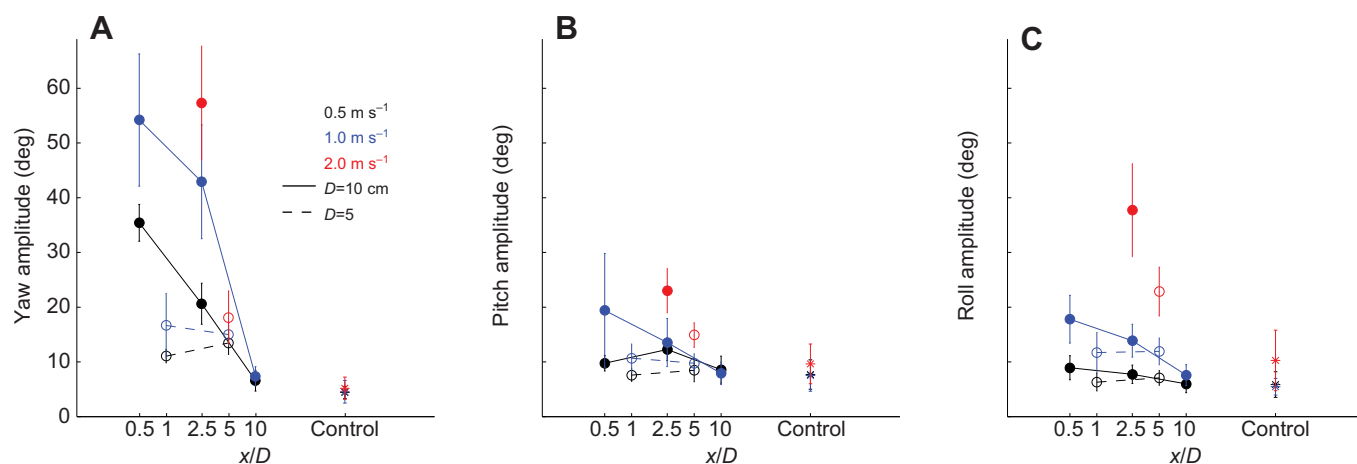

Fig. 5. Body oscillation amplitudes in yaw, pitch and roll experienced by hawkmoths flying in von Kármán vortex streets of varying vortex size, airspeed and downstream distance (*x/D*). Filled and open symbols represent the wakes from the large and small cylinder, respectively. Continuous and dashed lines represent the trend followed by the large and small cylinder data, respectively. Tested airspeeds are in red (2 m s^{-1}), blue (1 m s^{-1}) and black (0.5 m s^{-1}). Controls are represented by asterisks. (A) Yaw (ψ) *versus x/D*. (B) Pitch (θ) *versus x/D* and (C) roll (φ) *versus x/D*. Error bars represent ±1 s.d.
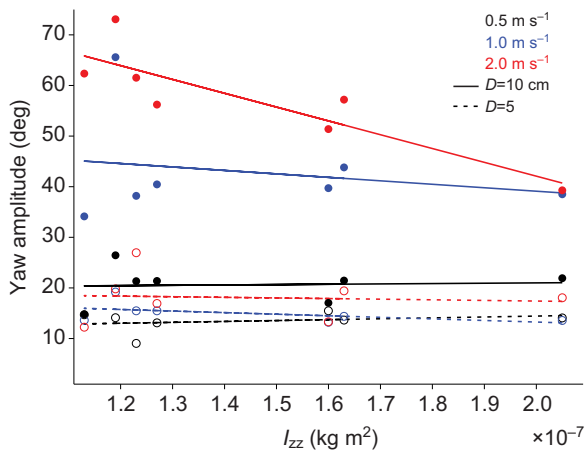
Fig. 6. Relationship between yaw oscillation amplitude ψ and yaw moment of inertia for different individual moths at x/D=2.5 (large cylinder) and 5 (small cylinder). Linear fits for the large cylinder: 0.5 m s^{-1}: $f(x)$=6.7×10^6x+19.7, R^2=0.004; 1 m s^{-1}: $f(x)$=−6.8×10^7x+52.8, R^2=0.05; 2 m s^{-1}: $f(x)$=−2.7×10^8x+96.7, R^2=0.76. Linear fits for the small cylinder: 0.5 m s^{-1}: $f(x)$=1.8×10^7x+10.9, R^2=0.08; 1 m s^{-1}: $f(x)$=−3.1×10^7x+19.5, R^2=0.25; 2 m s^{-1}: $f(x)$=−1.2×10^7x+19.9, R^2=0.01. Tested airspeeds are in red (2 m s^{-1}), blue (1 m s^{-1}) and black (0.5 m s^{-1}). Continuous and dashed lines represent the trend followed by the large and small cylinder data, respectively.

detrimental for yaw stabilization. In small vortices, the unaffected moth wing would produce a typical counter-torque response to an aerodynamically imposed body rotation (Hedrick et al., 2009). In contrast, in large vortices the two wings will both be within the vortex and thus the flow speed asymmetry that is the basis for flapping counter torque will not exist, making it more difficult to compensate for an imposed yaw velocity.

In fish, tail side-slips have been associated with the size of the vortex shedding. Tail beat amplitude of rainbow trout is highest when fish are freely swimming into a cylinder wake that is half of their body length (Liao et al., 2003b). Nevertheless, fish beat their tails at one-third lower rates in the large vortex wake than in freestream conditions. This is in contrast with our results, where all statistically significant changes in wingbeat frequency in the cylinder

wake were higher and the average wingbeat amplitude was unaffected by the treatments.

Flight stability *versus* vortex streets
The qualitative similarity of flight effects observed in hawkmoths flying in different wake regions was unexpected. For example, we initially hypothesized that the dominant retrograde streamwise flow in the near wake region (x/D <2) would produce pitch oscillations while locations further downstream where cross-stream flow fluctuations are stronger would produce roll or yaw oscillations. Instead, all flow perturbations produced similar responses, suggesting that the moth's dynamic stability and control properties play a large role in determining the outcome of these below wingbeat frequency events. For example, pitch may be controlled on a short time scale by the moth because it is found to be unstable in most control analyses of flapping flight (e.g. Taylor and Thomas, 2002; Sun and Xiong, 2005) and is also heavily involved in fore–aft maneuvers in hawkmoths (Cheng et al., 2011). Confirmation of the role of active control responses in determining the observed flight deviations will require additional experiments as our overall experimental approach was not designed to quantify or separate the effects of active, behavioral control responses from the aerodynamic effects (i.e. the physical interactions between flapping wings and flow).

Investigation of the performance of an open-loop mechanical or computational simulation of a flying moth exposed to a von Kármán street might reveal unexpected passive dynamic stability properties such as those described for a pyramid supported by an air column (Liu et al., 2012). However, direct investigation of neuromuscular activity in the presence of perturbation (e.g. Sponberg and Full, 2008) would be required to demonstrate active control. A combination of these approaches could reveal the contribution of active and passive responses to the overall flight behavior described here.

The large yaw and moderate roll effects observed in moths as compared with those observed in vortex street perturbations of hummingbirds (V.M.O.-J. et al., unpublished), which exhibit smaller oscillations in general, and bees (Ravi et al., 2013), which exhibit larger roll than yaw deviations, could be explained by morphology. Insects in flight might be affected by moderate fluid perturbations
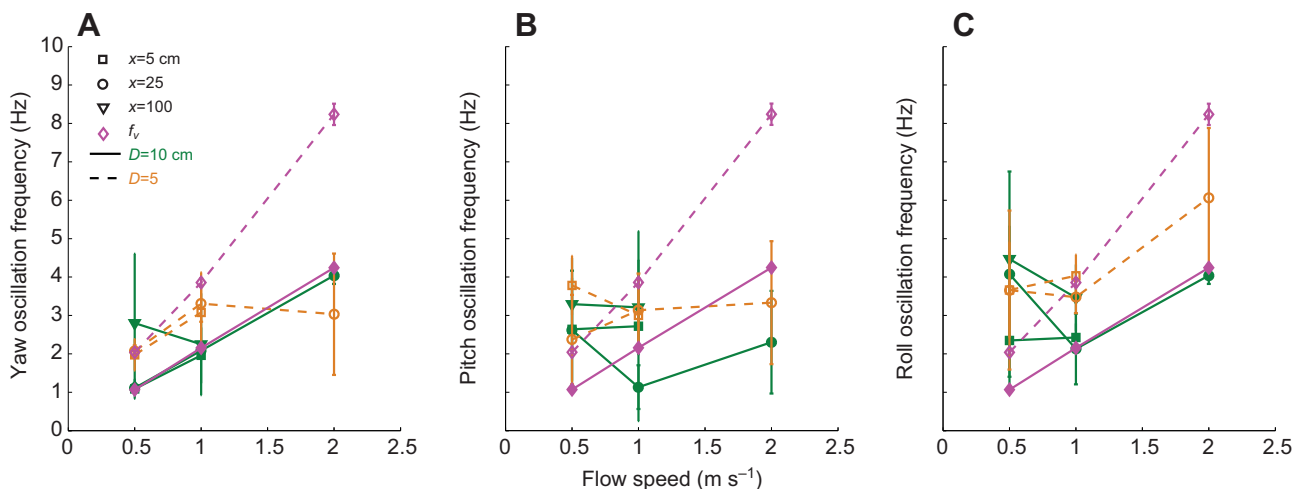

Fig. 7. Yaw, pitch and roll oscillation frequencies *versus* airspeed. Open orange symbols and dashed lines represent small cylinders. Filled green symbols and continuous lines represent large cylinders. Squares, circles and triangles represent downstream distances of 5, 25 and 100 cm, respectively. The vortex shedding frequency is represented by purple diamonds (open diamonds, small cylinder; filled diamonds, large cylinder). (A) Yaw (ψ) oscillation frequencies *versus* airspeed. (B) Pitch (θ) oscillation frequencies *versus* airspeed. (C) Roll (φ) oscillation frequencies *versus* airspeed. Error bars represent ±1 s.d.
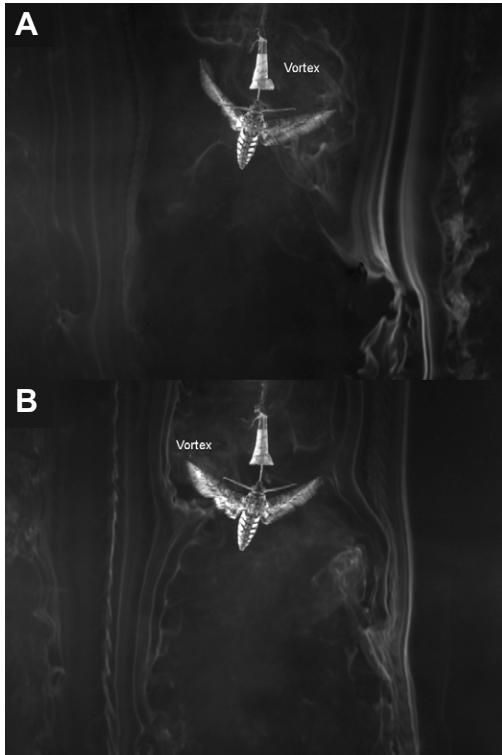
Fig. 8. Interaction between a vortex wake and a free-flying hawkmoth. Images are individual frames taken from smoke visualization videos of a hawkmoth flying 25 cm downstream of a large (A) and a small (B) cylinder wake at $1\,\mathrm{m\,s^{-1}}$. Large and small cylinders were 10 and 5 cm in diameter, respectively. Note that large vortices interact with both wings while the small vortices only interact with one wing. 'Curl' smoke structures at the side of the images were produced by the interaction of the air and the metal clamps connected to the hot-smoke wire. A gamma correction of 2.0 was applied to each video frame to enhance luminance.

because their rotational inertia, center of mass, wing configuration and nervous system enhance rapid control responses and maneuvers but reduce static stability (see Maynard Smith, 1952; Dudley, 2002). Lepidopteran species in particular often have relatively heavy wings, low wing loading, short abdomens and low wingbeat frequencies, but large aspect ratios compared with other insect species (Dudley, 2000) that make them susceptible to flow perturbations and also produce erratic flight. This makes the moths potentially more sensitive to environmental flows than bees or hummingbirds because the same environmental flow velocity will create larger aerodynamic forces and torques per unit moment of inertia in moths. Partially confirming this possibility, we observed that the amplitude of body displacements in yaw decreased with increasing moment of inertia, but only for moths flying at $2\,\mathrm{m\,s^{-1}}$ in the wake of the large cylinder. Differences among hawkmoths and bees may also be due to differences in experimental details: the bees were flying forward through the vortex street to a feeding location while the hawkmoths (and hummingbirds) were holding position at a feeder. We do note that both hawkmoths and bees make use of legs in providing flight stability. Bees are known to extend their hind legs to improve roll stability (Combes and Dudley, 2009) and we observed that the hawkmoths commonly extended their fore-legs when flying in the large cylinder wakes at $2\,\mathrm{m\,s^{-1}}$ with the possible intention and occasional result of grabbing the feeder and gaining stability, providing an alternate practical route for hawkmoths to stabilize their flight in adverse feeding conditions.

Unlike the two insect species, hummingbirds have a tail, which potentially provides additional flight stability and might explain their smaller oscillation amplitudes when perturbed by a vortex street.

Vortex decay

As we predicted, moth kinematic responses declined with downstream distance. These responses were qualitatively similar in different vortex wake regions, but response magnitudes declined as downstream distance increased and vortex strength concomitantly declined. At $x/D=10$, those effects practically disappeared. In contrast, smaller von Kármán vortices (i.e. vortex size smaller than a wing span) produced pitch and yaw responses that matched the vortex shedding frequency at all speeds, except at $2\,\mathrm{m\,s^{-1}}$; meanwhile, roll was only synchronized at $1\,\mathrm{m\,s^{-1}}$. All these responses, nevertheless, were smaller than those elicited by the large cylinder at all air speeds and downstream distances. This decline in flight disturbances can be explained taking into account the natural and abrupt decay of von Kármán streets at high Re and with increasing downstream distance (Williamson, 1996).

Metabolic implications

The metabolic implications of locomotion in unsteady environments have received little study compared with steady-state locomotor costs. Furthermore, the evidence is mixed on whether unsteady environments decrease or reduce costs. In human locomotion, uneven terrain has typically been found to increase costs (e.g. Voloshina, 2013). In fish swimming, turbulent flow has been found to increase the metabolic expenditures in some cases (Enders et al., 2003), but is associated with reduced muscle activation and likely reduced metabolic expenditure in others (Liao et al., 2003a). While there are no direct measurements of the metabolic expenditures of animals flying in unsteady flows published at this time, data from animals flying in groups provide some insight as animals in groups must accommodate the flows created by their neighbors. However, evidence is mixed here as well. Heart rate measurements from pelicans demonstrate a metabolic benefit to formation flight (Weimerskirch et al., 2001), while kinematic measurements from pigeons indicate that flocking flight is more costly for those animals (Usherwood et al., 2011). While we made no metabolic or muscle activity measurements of the moths, the increase in flapping frequency exhibited by moths flying in the vortex street (Fig. 4, Tables 3, 4) suggests that the unsteady flow has increased metabolic costs because flapping frequency is strongly associated with energy expenditure in animal flight (e.g. Ward et al., 2001). It is unclear what factors determine whether unsteady flows increase or reduce metabolic expenditure during locomotion in fluids, but we speculate that because the moths must stay in position at the feeder to avoid reduction in food intake similar to that due to flower oscillation (Sprayberry and Daniel, 2007), they are prevented from flying in a favorable location in the vortex street. In contrast, rainbow trout swimming with no restriction to movement assume a favorable position with respect to the cylinder or move in synchrony with the vortex wake, reducing the energetic requirement for swimming (Liao et al., 2003b).

Flow characteristics and tracking

Smoke visualization of the von Kármán vortices revealed secondary instabilities and turbulence for all wakes generated in the present study (Fig. 9). These observations agree with previous studies of von Kármán wakes in similar flow regimes (Williamson, 1996; Prasad and Williamson, 1997). The Strouhal number during our experiments was 0.21, which is a good match to the classical

Fig. 9. Smoke visualization to the vortex wake of a 5 cm diameter cylinder at 1 m s^{-1}. Note the secondary instabilities ('curls') in the wake.

experiments on cylinder wakes under similar Re (Williamson, 1996). Similarly, our observations of the rapid decay of the vortex shedding with distance agree with anterior visualizations of the far wake produced by a circular cylinder at Re ~10^3 (Cimbala et al., 1988).

We used the oscillating bird feather with the intent of tracking, in real time, the variations of the vortex wakes and the moth, having first used smoke visualization to determine that the feather tracks the vortices (supplementary material Movie 5). The f_F for the large and small cylinders was 10 and 50% lower than f_v at higher speeds, respectively. Thus, the feather technique or similar passive vortex tracking methods could be used in examining large vortex perturbations under field conditions where it is difficult to employ the smoke-wire method.

Ecology
Finally, our experiments demonstrate kinematic effects on moths flying in a von Kármán vortex street, potentially reducing nectar feeding efficiency. Moths might have difficulty feeding from flower in foraging areas characterized by large vortices and winds speeds higher than 2 m s^{-1}. Nectar feeding is an important activity for adult moths because this extra energy contributes to mating and egg production (O'Brien et al., 2000), so the capacity of moths to deal with flow disturbances may influence moth fitness. Environmental flows could affect moths in other ways. Moths use visual and olfactory clues to discern between flowers of different nectar content (Raguso and Willis, 2005; von Arx et al., 2012), and this capability can also be influenced by airflow turbulence. Field observations are required to determine the importance of these factors to wild moths and in general for nectar feeders.

Flow disturbances are also known to influence the departure time of migratory moths (Alerstam et al., 2011). However, these environmental flows also likely enable rapid and controlled migration by insects, to the extent that they achieve ground speeds and travel directions similar to those of passerine birds. This indicates that the flight capabilities of moths in dealing with and even taking advantage of strong and turbulent winds currents are still not well understood and are worth further investigation.

Conclusions
We demonstrated experimentally that kinematic effects experienced by *M. sexta* flying into von Kármán vortices are vortex size and frequency dependent, and are reduced dramatically with downstream distance, particularly for vortices larger than a wingspan. The moths exhibited the greatest effect on yaw orientation while roll orientation was affected at higher flight speeds. Pitch orientation was little affected and all these kinematic effects were consistent among different regions in the von Kármán street. Finally, vortex perturbations reduced maximum flight speeds compared with moths flying in unmodified wind tunnel flows.

APPENDIX
Wind tunnel characteristics
Wind tunnel design, construction and location
The low-speed wind tunnel used here (Fig. A1) is located in Wilson Hall at UNC-CH. It was designed in-house with final design details and construction by Quate Industrial Fabrication (Durham, NC, USA). It is a suction-type, open-flow wind tunnel, constructed mainly of 5 mm thick aluminum, and is housed in an 8.08×2.53×3.59 m (length × width × height) rectangular room where it is supported by a metal frame on locking wheels. With its current configuration, it has a minimum/maximum speed of 0.1/4 m s^{-1}. Air enters the square settling chamber and passes through a flow collimator and two screens. Air then enters a nozzle with a square entrance and a regular octagonal exit. The nozzle speeds up the air, which then passes through a plastic screen as it enters the working section. After leaving the working section, the air enters an expansion duct with an octagonal opening and circular exit. It then travels through a vibration-isolating duct, which also houses a flow collimator positioned directly in front of the fan entrance. Finally, the air passes through the fan and exits the wind tunnel through a discharge guard.

Settling chamber
In the settling chamber, a flow collimator and screens even out flow velocity where it is lowest (and thus resistance is minimal). The flow collimator chiefly parallelizes flow pathlines and reduces small-scale turbulence, while the screens chiefly create a more uniform speed profile and thin the boundary layer (Barlow et al., 1999; Mehta and Bradshaw, 1979). The settling chamber has interior dimensions of 153.5×153.5 cm. The inlet has 32.5 cm clearance with the floor and 45 cm clearance with the closest ceiling fixture (156 cm with the ceiling). The entrance to the settling chamber is curved in a circular arc. A recess in the settling chamber walls, together with a metal grid that spans the entrance, holds the flow collimator in place. The flow collimator is a 10.2 cm deep aluminum honeycomb (HexWeb ACG, Hexcel Co., Stamford, CT, USA), with >95% open
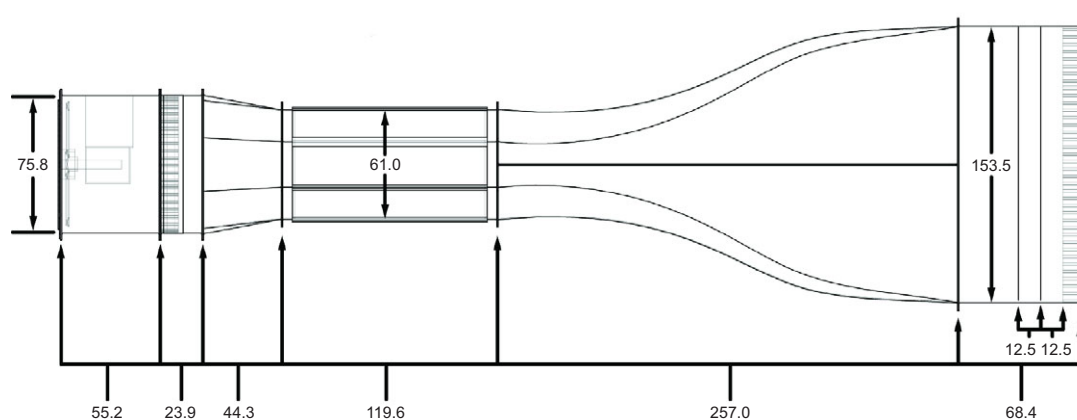
Fig. A1. A lateral view of the wind tunnel, shown without supporting structure. Dimensions are in centimeters. Some details intentionally excluded; honeycomb cell size not to scale.

area and a cell apothem of 4.75 mm. Next, the flow encounters two stainless steel woven mesh screens (Newark Wire Cloth Co., Clifton, NJ, USA), each with 36% open area and metal wire diameters of 254 and 25.4 µm, respectively. The finer screen was placed upstream in this study, opposite their typical operational order. The settling chamber attaches to the nozzle *via* hinges and clamps to allow rotation away from the rest of the wind tunnel. The side of this chamber is removable for screen cleaning purposes.

Nozzle

After the air exits the settling chamber, it then travels through the nozzle. The nozzle contracts to increase flow velocity, reduce velocity variations to a smaller fraction of the average velocity, and induce/maintain a well-defined, thin boundary layer (Barlow et al., 1999; Mehta and Bradshaw, 1979; Schlichting and Gersten, 2004). The nozzle is composed of two largely identical halves, shown in Fig. A1. The nozzle has a contraction ratio of ~5.7. The quadrilateral nozzle entrance maximizes contraction ratio given the room shape, while four chamfers at each edge expand to give the exit a regular octagonal shape. The octagonal shape is intended to thin the boundary layer and prevent flow separation near the edges (Barlow et al., 1999). The four interior chamfer hypotenuses from $x=1$ to 257 cm are described by:

$$\text{Hypotenuse} = -1.5365\text{e}-010x^4 - 4.3531\text{e}-007x^3 + 7.6242\text{e}-005x^2 + 0.11133x + 0.51218 . \quad \text{(A1)}$$

The other (horizontal and vertical) sides of the nozzle vary from $x=1$ to 120 cm as:

$$\text{Sides} = -4.6226\text{e}-007x^4 + 8.0989\text{e}-005x^3 - 0.0066144x^2 - 0.093549x + 153.2122 , \quad \text{(A2)}$$

and from $x=120$ to 257 cm as:

$$\text{Sides} = 1.2824\text{e}-007x^4 - 1.0414\text{e}-004x^3 + 0.036188x^2 - 6.4184x + 492.50 . \quad \text{(A3)}$$

Working section

The next destination for the flow is the working section, which is the portion of the wind tunnel designed for low-turbulence flow experiments. After exiting the nozzle (in the current experimental setup), the air passes through a plastic screen with >93% open area and a variable wire diameter of ~0.2–0.5 mm (1.27 cm per grid). In this experiment, this screen restricted moths to the working section, expansion duct and vibration isolator. The octagonal, transparent

design of the working section allows for viewing from eight different principal angles. It also allows for easier transition into the circular shape of the fan. The clear panels are made of Lexan (SABIC Innovative Plastics Holding BV, Pittsfield, MA, USA).

Expansion duct and vibration isolator

Expansion ducts and anti-twist vanes are typical wind tunnel components that decrease fan power requirements and reduce flow irregularities in upwind working sections (Barlow et al., 1999). This wind tunnel also has a vibration isolator. The expansion duct, which has an expansion ratio of ~1.0870, connects the working section to the vibration isolator. Next, the vibration isolator connects the expansion duct to the fan. Because of room size constraints, this wind tunnel's expansion duct is proportionally shorter than those of most similarly sized low-speed wind tunnels (Barlow et al., 1999); the vibration isolator helps create more laminar working section flow by increasing the distance between the working section and fan blades. This vibration isolator is the same diameter as the fan, and has the appearance of a flanged pipe with the middle section removed (Fig. A1). A ~0.5 mm thick tarp encircles the gap between the two flanged halves, and pipe clamps on either side of the gap secure the tarp in place. The support structure for the fan and downstream half of the vibration isolator is separable from that of the rest of the wind tunnel (although in this study, the two support structures were rigidly attached *via* metal tubing). The vibration isolator also houses a circular section of honeycomb flow collimator. This flow collimator (of the same material as previously described) is intended to damp the rotational patterns the fan introduces to the air. Thus, this collimator is intended to take the place of the anti-twist vanes typically situated directly before fan blades in similar wind tunnels (Barlow et al., 1999).

Fan and motor

The final section of the wind tunnel is the fan. Todd Air Solutions (Salisbury, NC, USA) delivered the 736 rpm, 1.49 kW, 0.165 m^3 s^{-1}, belt-driven tube axial duct fan (WAF-30, Cincinnati Fan & Ventilator Co., Mason, OH, USA). Situated parallel to the flow, two large steel plate fins and a teardrop belt tube collectively support the fan bearing encasement (which is not tapered). The power supply is 200 V, 15 A. This electricity runs through a safety circuit breaker and then a variable frequency drive (VS1MX82-2F, Baldor Electric Co., Fort Smith, AR, USA), which provides variable power to the fan motor (EM3558T-8, Baldor Electric Co.) and is controlled *via* an in-house dial-type potentiometer and switch panel. Flow finally

exits the wind tunnel by passing through a concentric circle discharge guard. The fan is 1.64 m from the room exit door and has between 0.65 and 1.07 m lateral clearance with the left and right walls of the room, respectively.

LIST OF SYMBOLS AND ABBREVIATIONS

3D	three-dimensional
b	wingspan
D	cylinder diameter
DLT	direct linear transformation
f_b	body oscillation frequency
f_F	feather oscillation frequency
f_v	vortex shedding frequency
l_b	body length
m_b	body mass
p_x, p_y	pixel coordinates
Re	Reynolds number
R_w	wing length
S_1	one-wing area
St	Strouhal number
U	airspeed
x	downstream distance from cylinder
η_w	wingbeat frequency
θ	pitch oscillation amplitude
υ	kinematic viscosity
ϕ	roll oscillation amplitude
φ_A	wingbeat amplitude
ψ	yaw oscillation amplitude

REFERENCES

Abdel-Aziz, Y. I. and Karara, H. M. (1971). Direct linear transformation into object space coordinates in close-range photogrammetry. In *Proceedings of the Symposium on Close-Range Photogrammetry*, pp. 1-18. Urbana-Champaign, IL: University of Illinois.

Alerstam, T., Chapman, J. W., Bäckman, J., Smith, A. D., Karlsson, H., Nilsson, C., Reynolds, D. R., Klaassen, R. H. and Hill, J. K. (2011). Convergent patterns of long-distance nocturnal migration in noctuid moths and passerine birds. *Proc. Biol. Sci.* **278**, 3074-3080.

Barlow, J. B., Rae, W. H. and Pope, A. (1999). *Low-Speed Wind Tunnel Testing.* New York, NY: Wiley & Sons, Inc.

Cheng, B., Deng, X. and Hedrick, T. L. (2011). The mechanics and control of pitching manoeuvres in a freely flying hawkmoth (*Manduca sexta*). *J. Exp. Biol.* **214**, 4092-4106.

Chopra, K. P. and Hubert, L. F. (1965). Mesoscale eddies in wakes of islands. *J. Atmos. Sci.* **22**, 652-657.

Cimbala, J. M., Nagib, H. M. and Roshko, A. (1988). Large structure in the far wakes of two-dimensional bluff bodies. *J. Fluid Mech.* **190**, 265-298.

Combes, S. A. and Dudley, R. (2009). Turbulence-driven instabilities limit insect flight performance. *Proc. Natl. Acad. Sci. USA* **106**, 9105-9108.

Dritcshel, D. G., Juarez, M. T. and Ambaum, M. H. P. (1999). The three-dimensional vortical nature of atmospheric and oceanic turbulent flows. *Phys. Fluids* **11**, 1512-1520.

Dudley, R. (2000). *The Biomechanics of Insect Flight: Form, Function, Evolution.* Princeton, NJ: Princeton University Press.

Dudley, R. (2002). Mechanisms and implications of animal flight maneuverability. *Integr. Comp. Biol.* **42**, 135-140.

Enders, E. C., Boisclair, D. and Roy, A. G. (2003). The effect of turbulence on the cost of swimming for juvenile Atlantic salmon (*Salmo salar*). *Can. J. Fish. Aquat. Sci.* **60**, 1149-1160.

Hedrick, T. L. (2008). Software techniques for two- and three-dimensional kinematic measurements of biological and biomimetic systems. *Bioinspir. Biomim.* **3**, 034001.

Hedrick, T. L., Cheng, B. and Deng, X. (2009). Wingbeat time and the scaling of passive rotational damping in flapping flight. *Science* **324**, 252-255.

Hedrick, T. L. (2011). Damping in flapping flight and its implications for manoeuvring, scaling and evolution. *J. Exp. Biol.* **214**, 4073-4081.

Ho, C. M. and Huerre, P. (1984). Perturbed free shear layers. *Annu. Rev. Fluid Mech.* **16**, 365-422.

Kawamura, T., Hiwada, M., Hibino, T., Mabuchi, I. and Kumada, M. (1984). Flow around a finite circular cylinder on a flat plate (cylinder height greater than turbulent boundary layer thickness). *Bull. JSME* **27**, 2142-2151.

Liao, J. C. (2007). A review of fish swimming mechanics and behaviour in altered flows. *Philos. Trans. R. Soc. B* **362**, 1973-1993.

Liao, J. C., Beal, D. N., Lauder, G. V. and Triantafyllou, M. S. (2003a). Fish exploiting vortices decrease muscle activity. *Science* **302**, 1566-1569.

Liao, J. C., Beal, D. N., Lauder, G. V. and Triantafyllou, M. S. (2003b). The Kármán gait: novel body kinematics of rainbow trout swimming in a vortex street. *J. Exp. Biol.* **206**, 1059-1073.

Liu, B., Ristroph, L., Weathers, A., Childress, S. and Zhang, J. (2012). Intrinsic stability of a body hovering in an oscillating airflow. *Phys. Rev. Lett.* **108**, 068103.

Marzkirch, W. (1987). *Flow Visualization*, 2nd edn. London: Academic Press.

Maynard Smith, J. (1952). The importance of the nervous system in the evolution of animal flight. *Evolution* **6**, 127-129.

Mehta, R. D. and Bradshaw, P. (1979). Design rules for small low speed wind tunnels. *Aeronaut. J.* **83**, 443-449.

O'Brien, D. M., Schrag, D. P. and del Rio, C. M. (2000). Allocation to reproduction in a hawkmoth: a quantitative analysis using stable carbon isotopes. *Ecology* **81**, 2822-2831.

Okamoto, S. and Sunabashiri, Y. (1992). Vortex shedding from a circular cylinder of finite length placed on a ground plane. *J. Fluids Eng.* **114**, 512-521.

Parnaudeau, P., Carlier, J., Heitz, D. and Lamballais, E. (2008). Experimental and numerical studies of the flow over a circular cylinder at Reynolds number 3900. *Phys. Fluids* **20**, 085101.

Poggi, D., Porporato, A., Ridolfi, L., Albertson, J. D. and Katul, G. G. (2004). The effect of vegetation density on canopy sub-layer turbulence. *Boundary-Layer Meteorology* **111**, 565-587.

Prasad, A. and Williamson, C. H. K. (1997). Three-dimensional effects on turbulent bluff-body wakes. *J. Fluid Mech.* **343**, 235-265.

Raguso, R. A. and Willis, M. A. (2005). Synergy between visual and olfactory cues in nectar feeding by naïve hawkmoths, *Manduca sexta*. *Anim. Behav.* **69**, 407-418.

Ravi, S., Crall, J., Fisher, A. and Combes, S. (2013). Rolling with the flow: bumblebees flying in unsteady wakes. *J. Exp. Biol.* **216**, 4299-4309.

Sponberg, S. and Full, R. J. (2008). Neuromechanical response of musculo-skeletal structures in cockroaches during rapid running on rough terrain. *J. Exp. Biol.* **211**, 433-446.

Sprayberry, J. D. H. and Daniel, T. L. (2007). Flower tracking in hawkmoths: behavior and energetics. *J. Exp. Biol.* **210**, 37-45.

Schlichting, H. and Gersten, K. (2004). *Boundary-Layer Theory*, 8th edn. New York, NY: Springer.

Sun, M. and Xiong, Y. (2005). Dynamic flight stability of a hovering bumblebee. *J. Exp. Biol.* **208**, 447-459.

Taylor, G. K. and Thomas, A. L. R. (2002). Animal flight dynamics II. Longitudinal stability in flapping flight. *J. Theor. Biol.* **214**, 351-370.

Usherwood, J. R., Stavrou, M., Lowe, J. C., Roskilly, K. and Wilson, A. M. (2011). Flying in a flock comes at a cost in pigeons. *Nature* **474**, 494-497.

Vogel, S. (1994). *Life in Moving Fluids: the Physical Biology of Flow*. Princeton, NJ: Princeton University Press.

von Arx, M., Goyret, J., Davidowitz, G. and Raguso, R. A. (2012). Floral humidity as a reliable sensory cue for profitability assessment by nectar-foraging hawkmoths. *Proc. Natl. Acad. Sci. USA* **109**, 9471-9476.

Voloshina, A. S., Kuo, A. D., Daley, M. A. and Ferris, D. P. (2013). Biomechanics and energetics of walking on uneven terrain. *J. Exp. Biol.* **216**, 3963-3970.

Ward, S., Möller, U., Rayner, J. M. V., Jackson, D. M., Bilo, D., Nachtigall, W. and Speakman, J. R. (2001). Metabolic power, mechanical power and efficiency during wind tunnel flight by the European starling *Sturnus vulgaris*. *J. Exp. Biol.* **204**, 3311-3322.

Webb, P. W. (1998). Entrainment by river chub nocomis micropogon and smallmouth bass *Micropterus dolomieu* on cylinders. *J. Exp. Biol.* **201**, 2403-2412.

Weimerskirch, H., Martin, J., Clerquin, Y., Alexandre, P. and Jiraskova, S. (2001). Energy saving in flight formation. *Nature* **413**, 697-698.

Williamson, C. H. K. (1996). Vortex dynamics in the cylinder wake. *Annu. Rev. Fluid Mech.* **28**, 477-539.